Acta Crystallographica Section D
Biological Crystallography
ISSN 1399-0047

Structural and functional characterization of an Isd-type haem-degradation enzyme from *Listeria monocytogenes*

Thao Duong, Kwangsu Park, Truc Kim, Sung Wook Kang, Myung Joon Hahn, Hye-Yeon Hwang and Kyeong Kyu Kim*

Department of Molecular Cell Biology, Samsung Biomedical Research Institute, Sungkyunkwan University School of Medicine, Suwon 440-746, Republic of Korea

Correspondence e-mail: kyeongkyu@skku.edu

Received 17 June 2013
Accepted 8 November 2013

PDB reference: Isd-LmHde, 4kia

Bacterial pathogens have evolved diverse types of efficient machinery to acquire haem, the most abundant source of iron in the human body, and degrade it for the utilization of iron. Gram-positive bacteria commonly encode IsdG-family proteins as haem-degrading monooxygenases. *Listeria monocytogenes* is predicted to possess an IsdG-type protein (Lmo2213), but the residues involved in haem monooxygenase activity are not well conserved and there is an extra N-terminal domain in Lmo2213. Therefore, its function and mechanism of action cannot be predicted. In this study, the crystal structure of Lmo2213 was determined at 1.75 Å resolution and its haem-binding and haem-degradation activities were confirmed. Structure-based mutational and functional assays of this protein, designated as an Isd-type *L. monocytogenes* haem-degrading enzyme (Isd-LmHde), identified that Glu71, Tyr87 and Trp129 play important roles in haem degradation and that the N-terminal domain is also critical for its haem-degrading activity. The haem-degradation product of Isd-LmHde is verified to be biliverdin, which is also known to be the degradation product of other bacterial haem oxygenases. This study, the first structural and functional report of the haem-degradation system in *L. monocytogenes*, sheds light on the concealed haem-utilization system in this life-threatening human pathogen.

1. Introduction

Iron is necessary for many important metabolic pathways in living organisms. Many bacterial pathogens also need iron for pathogenesis and infection. Thus, they have developed various iron-uptake systems to acquire iron from their surroundings. Iron is abundantly present as haem in mammalian cells, and thus pathogenic bacteria harbour various systems to acquire haem from their host to survive and cause disease. In Gram-positive bacteria, two distinct haem-acquisition systems have been identified: (i) the iron-regulated surface determinant (Isd) system and (ii) the haem-transport system (Hts). In these pathways, haem degradation catalyzed by a haem oxygenase is a pivotal step in releasing iron from haem for nutrient requirements (Hammer & Skaar, 2011). Furthermore, haem degradation is also necessary to avoid haem toxicity in bacteria (Anzaldi & Skaar, 2010).

Bacterial haem oxygenases can be categorized into three major families based on their structures (Reniere *et al.*, 2007): the haem oxygenase (HO)-like family (Wilks & Schmitt, 1998), the ChuS family (Suits *et al.*, 2005) and the IsdG family (Skaar *et al.*, 2004; Wu *et al.*, 2005). The HO-like family has been identified in both Gram-positive bacteria (Wilks & Schmitt, 1998) and Gram-negative bacteria (Schuller *et al.*,

2001), whereas the ChuS family has only been found in Gram-negative bacteria (Suits *et al.*, 2005). The IsdG family is also present in both Gram-positive bacteria (Skaar *et al.*, 2004) and Gram-negative bacteria (Puri & O'Brian, 2006).

The HO-like family proteins exist as monomers harbouring a helical bundle domain with a G*XXX*G motif that is required for catalytic activity. Biliverdin, carbon monoxide (CO) and free iron are released from haem degradation by HO-like family proteins (Wilks & Schmitt, 1998; Schuller *et al.*, 1999). Haem is degraded *via* three successive oxygenation steps: the α-*meso* C atom of the porphyrin ring is selectively oxygenated to α-*meso*-hydroxyhaem, verdohaem is then generated as the reaction intermediate with the concomitant generation of CO, and finally the ring of verdohaem is opened to form biliverdin and release iron (Unno *et al.*, 2007, 2012). The ChuS family proteins show no sequential or structural similarity to the HO-like family proteins, but produce the same haem-degradation products as HO-like family proteins (Suits *et al.*, 2005). ChuS family proteins are monomeric enzymes comprising two large pleated β-sheets (Suits *et al.*, 2005). PhuS from *Pseudomonas aeruginosa*, which belongs to the ChuS family proteins, has exceptionally been proposed to deliver haem rather than to degrade haem (Lansky *et al.*, 2006). The IsdG family proteins are different from the HO-like and ChuS family proteins in terms of structure and the mechanism of haem degradation; they form a homodimeric β-barrel fold containing two separate active sites with an Asn-Trp-His catalytic triad (Wu *et al.*, 2005). Most distinctively, IsdG has a distorted haem, which is a prerequisite for haem degradation, while the HO-like and ChuS family proteins harbour a planar haem (Lee *et al.*, 2008). It is also worth noting that IsdG and IsdI from *Staphylococcus aureus* degrade haem to a novel chromophore (staphylobilin) that is distinct from biliverdin (Reniere *et al.*, 2010), producing formaldehyde rather than CO (Matsui *et al.*, 2013), which suggests that the haem-degrading mechanisms of IsdG and other haem oxygenases differ. It has recently been reported that MhuD from *Mycobacterium tuberculosis*, which belongs to the IsdG family proteins, degrades haem to a novel chromophore (mycobilin) without the liberation of CO (Nambu *et al.*, 2013).

Recently, two haem-degrading monooxygenases, namely HmoA and HmoB, were identified in *Bacillus subtilis* (Gaballa & Helmann, 2011). HmoB belongs to the IsdG family since the C-terminal domain of HmoB has high sequential and structural homology to full-length IsdG (Gaballa & Helmann, 2011). However, HmoA shows marginal sequential homology with IsdG and thus is characterized as a divergent member of the IsdG family. Similarly to IsdG family proteins, HmoB is able to degrade haem and release iron, but its degradation product and reaction mechanism have not yet been well characterized (Gaballa & Helmann, 2011). In addition, HmoB possesses an extra N-terminal domain whose function is unknown (Park *et al.*, 2012). These observations suggest diverse haem-degradation mechanisms for IsdG family proteins; however, no detailed mechanism is available to date.

Listeria monocytogenes, a Gram-positive nonsporulating motile rod, is one of the most important human pathogens and causes severe diseases such as listeriosis (Farber & Peterkin, 1991). The manifestations of listeriosis include septicaemia, meningitis (Gray, 1962), encephalitis (Armstrong & Fung, 1993), corneal ulcers (Holland *et al.*, 1987), pneumonia (Whitelock-Jones *et al.*, 1989) and intrauterine or cervical infections in pregnant women resulting in spontaneous abortion or stillbirth (Rabau & David, 1962). Similarly to the case in other pathogenic bacteria, acquisition of iron by *L. monocytogenes* is indispensable for its viability and pathogenicity (Newton *et al.*, 2005; Sword, 1966; Conte *et al.*, 1996). In an iron-limited environment, *L. monocytogenes* has been shown to modulate a variety of iron-uptake systems such as a citrate-inducible receptor of ferric citrate (Adams *et al.*, 1990), siderophores, catechol siderophore-like molecules (Simon *et al.*, 1995), a cell-surface transferrin-binding protein (Hartford *et al.*, 1993) and ABC transporters acquiring ferric hydroxamates (Fhu) or haemin/haemoglobin (Hup) (Jin *et al.*, 2006). Haem degradation is a critical step for haem utilization, but few studies of haem utilization in this organism have been conducted. In the genomic database of *L. monocytogenes*, only IsdG has been identified as a haem oxygenase; no other haem-degradation enzymes have been annotated. Considering the requirement for iron and haem for the survival and infection of *L. monocytogenes*, additional haem-degradation machineries are likely to be present in this organism.

In this study, we performed bioinformatic analysis of the genomic data of *L. monocytogenes* and identified Lmo2213 as a putative haem-degrading enzyme. Using structural and functional analyses, we proved that Lmo2213 degrades haem and we thus renamed Lmo2213 as Isd-LmHde (IsdG-type *L. monocytogenes* haem-degrading enzyme). This is the first report of the structural and functional investigation of a haem-degradation enzyme from *L. monocytogenes*.

2. Materials and methods

2.1. Materials

All chemicals used in this study were purchased from Sigma (St Louis, Missouri, USA) unless otherwise specified. The strains and plasmids used in this study are listed in Supplementary Table S1.[1] *Escherichia coli* strains were grown in Luria–Bertani (LB) broth (Difco, Franklin Lakes, New Jersey, USA) at 37°C. To produce solid medium, 1.5% agar was added. The medium was supplemented with kanamycin to a final concentration of 30 μg ml^{-1} as needed.

2.2. Construction of the expression vector

The gene encoding Isd-LmHde was PCR-amplified from the genomic DNA of *L. monocytogenes* EGD-e (GenBank accession No. NC003210, gene ID 984794) using *Pfu* DNA polymerase (Stratagene, Santa Clara, California, USA) with the primers listed in Supplementary Table S2. The PCR product was digested with *Bam*HI and *Xho*I and isolated from

[1] Supporting information has been deposited in the IUCr electronic archive (Reference: MH5100).

Table 1
Data-collection and refinement statistics.

Values in parentheses are for the last resolution shell.

Data-collection statistics	
Space group	$P2_1$
Unit-cell parameters (Å, °)	a = 26.61, b = 59.47, c = 45.43, $\alpha = \gamma = 90$, $\beta = 94.57$
Wavelength (Å)	1.000
Resolution (Å)	50–1.75 (1.81–1.75)
$R_{\rm merge}$† (%)	6.4 (16.6)
Completeness (%)	99.1 (94.0)
No. of unique reflections	14209
Multiplicity	3.6 (3.0)
$\langle I/\sigma(I)\rangle$	30.41 (5.78)
Refinement statistics	
Resolution (Å)	45.29–1.75
$R_{\rm work}/R_{\rm free}$‡ (%)	19.1/24.4
No. of reflections	13479
No. of atoms	
Protein	1253
Water	177
B factor (Å^2)	16.24
R.m.s. deviations	
Bond lengths (Å)	0.015
Bond angles (°)	1.346
Ramachandran plot (%)	
Preferred regions	96.64
Allowed regions	3.36
Outliers	0.00

† $R_{\rm merge} = \sum_{hkl}\sum_i |I_i(hkl) - \langle I(hkl)\rangle|/\sum_{hkl}\sum_i I_i(hkl)$. ‡ $R = \sum_{hkl} \big||F_{\rm obs}| - |F_{\rm calc}|\big|/\sum_{hkl}|F_{\rm obs}|$.

an agarose gel using a Labo Pass gel-extraction kit (Cosmo Genetech, Seoul, Republic of Korea). The purified DNA was then ligated to the *Bam*HI/*Xho*I-digested pVFT1S vector (Korea Patent 1020050051893). The ligated vector was then introduced into *E. coli* strain DH5α (Novagen, Madison, Wisconsin, USA). The coding sequence of the cloned gene was confirmed by nucleotide sequencing. A similar procedure was used to generate a vector containing the gene coding for the C-terminal domain of Isd-LmHde (C-Isd-LmHde; residues 51–167), the HmoB protein from *B. subtilis* or the IsdG protein from *S. aureus* with the primers listed in Supplementary Table S2.

2.3. Protein preparation

Initially, selenomethionine (SeMet) substituted protein was produced for the purpose of phasing using the multiple anomalous dispersion (MAD) method. However, since the crystal structure of a structurally homologous protein had been reported during the crystallization experiment, we used molecular replacement for phasing with the diffraction data obtained from the crystal of the SeMet-substituted protein. The SeMet-substituted protein was expressed in *E. coli* B834 (DE3) (Novagen, Madison, Wisconsin, USA), a methionine-auxotrophic strain. Cells were grown at 37°C in M9 medium supplemented with 30 µg ml^{-1} kanamycin and 100 mg l^{-1} L-SeMet until the optical density at 600 nm (OD_{600}) reached 0.6. Isopropyl β-D-1-thiogalactopyranoside (IPTG) was added to a final concentration of 0.25 m*M* at 18°C for 24 h to induce protein expression. Cells were harvested and disrupted in buffer *A* (25 m*M* Tris–HCl pH 8.0, 0.5 *M* sodium chloride, 40 m*M* imidazole, 1 m*M* dithiothreitol) by sonication. The crude extract was loaded onto a HiTrap chelating column (GE Healthcare, Waukesha, Wisconsin, USA) and eluted with a linear gradient of 100–250 m*M* imidazole in buffer *A*. The fractions containing Isd-LmHde were dialyzed against buffer *B* (50 m*M* Tris–HCl pH 8.0, 150 m*M* sodium chloride, 1 m*M* ethylenediaminetetraacetic acid, 1 m*M* dithiothreitol) and the N-terminal His tag was removed using *Tobacco etch virus* (TEV) protease. The sample was loaded once more onto the HiTrap chelating column for removing the His tag. The flow-through from the HiTrap chelating column was concentrated and loaded onto a HiLoad 16/60 Superdex 75 gel-filtration column (GE Healthcare, Waukesha, Wisconsin, USA) which was pre-equilibrated with buffer *C* (25 m*M* sodium citrate pH 5.6, 50 m*M* ammonium sulfate, 1 m*M* dithiothreitol). Finally, purified Isd-LmHde was concentrated to 15 mg ml^{-1} for crystallization and stored at −70°C. For the biochemical assay, Isd-LmHde was purified in a similar way as the protein used for crystallization, but dithiothreitol was not added during purification and the N-terminal His tag was not removed. The C-terminal domain of Isd-LmHde (C-Isd-LmHde), HmoB and IsdG were also expressed and purified using a protocol similar to that used for wild-type Isd-LmHde.

2.4. Crystallization

Initial crystallization screening was performed using 15 mg ml^{-1} SeMet-substituted Isd-LmHde by the microbatch method under Al's Oil at 22°C with various crystal screening solutions such as Crystal Screen, Crystal Screen 2, Index, Wizard 1 and 2, Cryo 1 and 2, SaltRX 1 and 2 (Hampton Research, Aliso Viejo, California, USA; Emerald Bio, Bainbridge Island, Washington, USA). 1 µl screening solution and 1 µl protein solution were mixed and placed into each well of a Nunc 96-well Mini Tray (Nalge Nunc International, Rochester, New York, USA). Initially, needle-shaped crystals were obtained from a crystallization condition consisting of 0.2 *M* ammonium sulfate, 0.1 *M* bis-tris pH 5.5, 25% polyethylene glycol 3350. After optimization of the conditions, crystals with good diffraction quality were obtained from 25% polyethylene glycol 3350, 0.1 *M* sodium citrate pH 5.6, 0.2 *M* ammonium sulfate at 14°C.

2.5. Data collection and structure determination

X-ray diffraction data were collected from a crystal of SeMet-substituted protein with 99.1% completeness to 1.75 Å resolution at 100 K using an ADSC Quantum 315R CCD detector on beamline 38B1 of the Photon Factory, Japan. Data were processed and integrated using *DENZO* and scaled using *SCALEPACK* from the *HKL*-2000 suite (Otwinowski & Minor, 1997). The data sets revealed that the crystals belonged to the primitive monoclinic space group $P2_1$, with unit-cell parameters a = 26.61, b = 59.47, c = 45.43 Å, β = 94.57°. The crystal structure of Isd-LmHde was solved by the *MOLREP* molecular-replacement program (Vagin & Teplyakov, 2010) using an uncharacterized ferredoxin-fold protein (YP_014836.1; an antibiotic biosynthesis monooxygenase

from *L. monocytogenes* 4b F2365; PDB entry 3fez; Joint Center for Structural Genomics, unpublished work), as a search model. The *ARP*/*wARP* automated model-building program (Morris *et al.*, 2003) was employed to build the model, which was further manually adjusted with the *Coot* model-building program (Emsley & Cowtan, 2004) and iteratively refined with *REFMAC*5 (Murshudov *et al.*, 2011). The final model was validated using *Coot* and *PROCHECK* (Laskowski *et al.*, 1993). Data statistics for the synchrotron data collection and the refinement of the crystal structure are summarized in Table 1. All structural figures were generated using *PyMOL* (http://www.pymol.org).

2.6. Site-directed mutagenesis

The desired residues were individually substituted with Ala or Arg using the QuikChange site-directed mutagenesis kit (Agilent Technologies, Santa Clara, California, USA) according to the manufacturer's instructions with the primers listed in Supplementary Table S2. The mutant proteins were expressed and purified in the same way as the wild-type protein.

2.7. Haemin-binding assay

The binding of haemin to the protein was observed by the quenching of the intrinsic fluorescence of Trp in haem-binding buffer consisting of 50 m*M* Tris–HCl pH 8.0, 150 m*M* sodium chloride. The fluorescence measurements were carried out at room temperature using an FP-750 spectrofluorometer (Jasco, Tokyo, Japan) with excitation at 295 nm. 1 µ*M* haemin was added to 5 µ*M* protein in the haem-binding buffer up to 40 µ*M* haemin. Spectra were recorded 10 min after the addition of haemin.

2.8. Reconstitution of apo Isd-LmHde with haemin

Haemin stock solution (10 m*M*) was prepared by dissolving 3.3 mg haemin crystals in 250 µl 0.1 *M* NaOH followed by neutralization with 250 µl 1 *M* Tris–HCl pH 8.0. To reconstitute the protein–haemin complex, the haemin stock solution was added to 100 µ*M* apo Isd-LmHde in a 2:1 molar ratio at room temperature and was protected from light for 1 h. Excess haemin was removed using a disposable PD10 desalting column (GE Healthcare, Waukesha, Wisconsin, USA). Protein concentrations were determined by the Bradford assay (Bradford, 1976) using bovine serum albumin as a standard, and the haemin concentration was determined by the pyridine haemochrome method (Sinclair *et al.*, 2001).

2.9. Haemin-degradation assay

Degradation of haemin was monitored in the presence of 10 m*M* ascorbic acid as an electron donor in 50 m*M* Tris–HCl pH 8.0, 150 m*M* sodium chloride. The reduction in the Soret peak of the 10 µ*M* haemoprotein complex was monitored every 5 min for 30 min and after 2 h. The degradation assay was performed in the presence of catalase in a 0.5:1 molar ratio with the haemoprotein complex (Skaar *et al.*, 2004) to rule out the non-enzymatic degradation of haemin by hydrogen peroxide *via* a coupled oxidation reaction (Sigman *et al.*, 2001).

2.10. Mass spectrometry

The degradation product was purified by solid-phase extraction (SPE) using a spin column (C_{18} Ultra-Micro Spin Column, Harvard Apparatus, Holliston, Massachusetts, USA). The spin column was pre-wetted with 100 µl solvent *A* [20% methanol:80% water(*v*:*v*)] at 5000 rev min^{-1}, which was repeated three times. The sample containing the degradation product was dissolved in solvent *A* and then loaded onto the spin column. The spin column was washed with solvent *A* three times and eluted with solvent *B* (methanol). The degradation

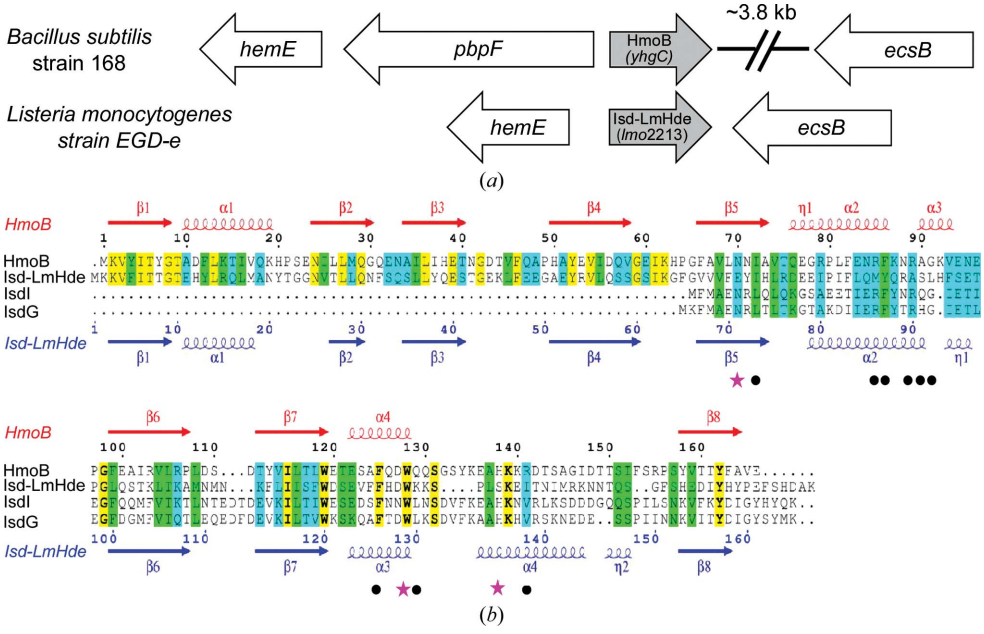

Figure 1
Sequence analyses of Isd-LmHde and its homologues. (*a*) Genomic structures of HmoB from *B. subtilis* and Isd-LmHde from *L. monocytogenes*. The name of each strain is denoted and the name of each gene is presented within each arrow-shaped box. The direction of each arrow-shaped box denotes the predicted direction of transcription. (*b*) Multiple sequence alignment of *B. subtilis* HmoB with *S. aureus* Isd-LmHde, IsdI and IsdG. The predicted secondary structures and residue numbers of HmoB and Isd-LmHde are shown above and below the alignment, respectively. Identical residues are boxed in yellow. Green and cyan boxes depict significantly and weakly conserved residues, respectively. The residues involved in haem binding in IsdG are denoted by black dots. The key residues that are critical for haem-degrading activity in IsdG are denoted by pink asterisks. Alignment was carried out using *ClustalW* (Thompson *et al.*, 1994) and the figure was adapted from the output of *ESPript* (Gouet *et al.*, 1999).

product was identified using matrix-assisted laser desorption/ionization–time-of-flight (MALDI–TOF) mass spectrometry (Autoflex Speed series; Bruker Daltonics, Leipzig, Germany). Mass spectra were acquired at 500 Hz in positive-ion reflection mode and were averaged over 1000 laser (355 nm, Nd:YAG laser) shots. A 2,5-dihydroxybenzoic acid (2,5-DHB; Aldrich, Seoul, Republic of Korea) matrix was used.

2.11. Carbon monoxide (CO) detection assay

The CO detection assay was performed as described by Nambu *et al.* (2013) with some modifications. Briefly, the haem-degradation reactions as described above for 100 µ*M* Isd-LmHde or HmoB were added to sealed vials. IsdG at a concentration of 0, 5, 10, 15, 20 and 40 µ*M* was also introduced to the reaction. After 1 h incubation, a mixture of myoglobin and sodium dithionite was injected to give final concentrations of 10 µ*M* and 10 m*M*, respectively, and incubated for 10 min at room temperature before opening the vials to measure the absorption spectra. A control spectrum was measured from the same reaction mixture before haem degradation.

3. Results

3.1. Bioinformatic analysis of Lmo2213 in *L. monocytogenes*

Genomic analyses of the *hmoB* locus in *B. subtilis* indicated that the *hmoB* gene is flanked by two different polycistronic

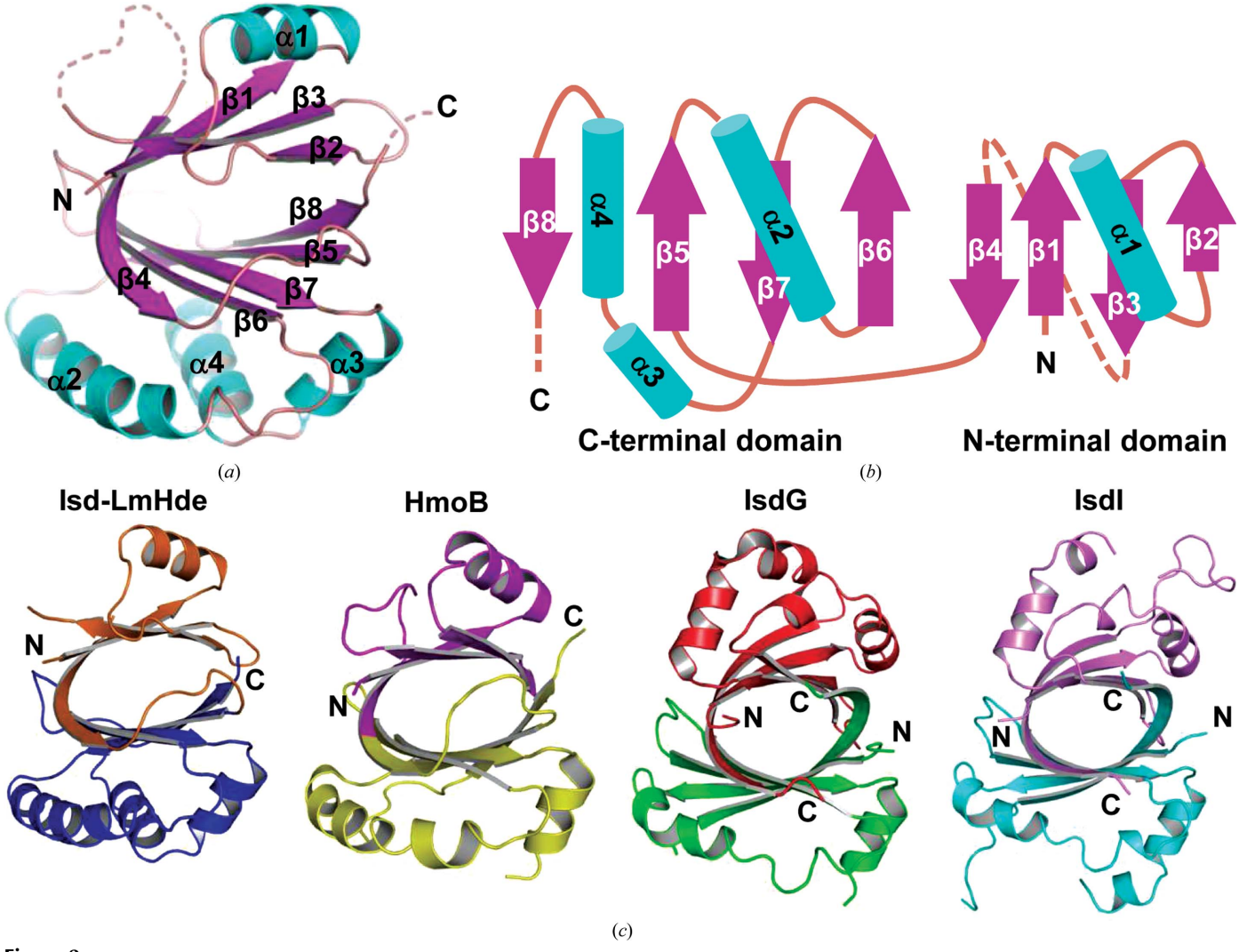

Figure 2
Overall structure of Isd-LmHde. (*a*) Ribbon diagram of Isd-LmHde. The N- and C-termini and the secondary-structure elements are labelled. The α-helices and β-strands are coloured cyan and magenta, respectively. The dashed curves represent the region that was not modelled (residues 44–49 and 161–167). (*b*) Cartoon representing the topology of the overall structure of Isd-LmHde. The α-helices and β-strands are represented by cyan cylinders and magenta arrows, respectively. The dashed curves represent the region that was not modelled (residues 44–49 and 161–167). The N- and C-termini and the secondary-structure elements are labelled. (*c*) Structural comparison of Isd-LmHde with other haem-degrading enzymes. Ribbon models of Isd-LmHde from *L. monocytogenes*, HmoB from *B. subtilis* (PDB entry 3tvz), IsdI from *S. aureus* (PDB entry 1sqe) and IsdG from *S. aureus* (PDB entry 1xbw) are compared in the same orientation. The N-terminal and C-terminal domains of Isd-LmHde are depicted in orange and blue, respectively. The N-terminal and C-terminal domains of HmoB are denoted in magenta and yellow, respectively. One subunit of IsdG is coloured green, while the other subunit is coloured red. One subunit of IsdI is coloured cyan, while the other subunit is coloured violet. The N- and C-termini of each monomer are labelled. The figure was prepared using *PyMOL* (http://www.pymol.org).

operons. Upstream *hmoB* is flanked by *hemE* encoding a ferrochelatase required for the final step of the haem-biosynthesis pathway, while downstream *hmoB* is flanked by *ecsB*, which encodes a putative ABC transporter (Fig. 1*a*). In addition, the gene locus and structure of *hmoB* are also conserved in other pathogenic Gram-positive bacteria belonging to the order Bacillales, such as *Listeria*, *Staphylococcus* and *Bacillus* (data not shown). In *L. monocytogenes*, the gene locus of *lmo2213* is similar to that of *B. subtilis hmoB* (Fig. 1*a*). The Lmo2213 protein has 25.3% sequence identity to *B. subtilis* HmoB, and its sequence identities to IsdG from *S. aureus* and HmoA from *B. subtilis* are 15.1 and 12.2%, respectively. However, the sequence identity between IsdG and Lmo2213 is 27.5% when the C-terminal domain of Lmo2213 is used for comparison. The Lmo2213 protein also showed a similar secondary structure to HmoB and IsdG when their secondary structures were compared using the *Jpred*3 prediction server (Cole *et al.*, 2008; data not shown). Therefore, further studies on IsdG or HmoB homologues in Bacillales are necessary to elucidate their biological roles and to understand the haem-utilization and haem-detoxification system in those Gram-positive pathogens. We hypothesized

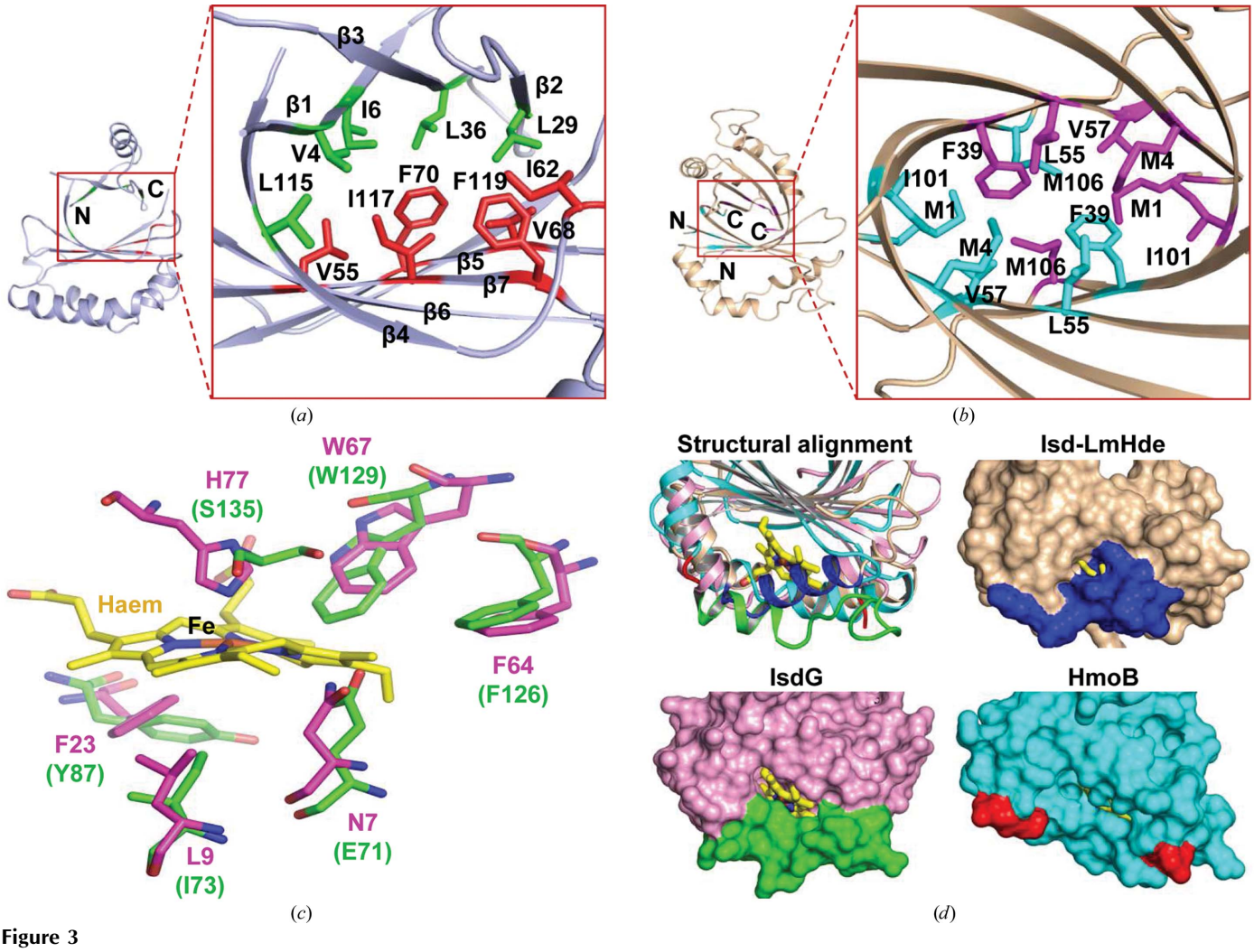

Figure 3
Hydrophobic interactions in the eight-stranded β-barrel of Isd-LmHde and dimeric IsdG and the putative haem-binding sites of Isd-LmHde. The residues involved in hydrophobic interactions in the eight-stranded β-barrel of (*a*) Isd-LmHde and (*b*) dimeric IsdG are depicted as stick models and labelled. The residues belonging to the N-terminal and C-terminal domains of Isd-LmHde are coloured green and red, respectively. The backbone of the remaining residues of Isd-LmHde is coloured light blue and the secondary-structure elements are labelled. The residues belonging to the subunits of IsdG are coloured magenta and cyan. The backbone of the remaining residues of dimeric IsdG is coloured wheat. The N- and C-termini of Isd-LmHde or each subunit of IsdG are labelled. (*c*) A putative haem-binding site in Isd-LmHde. The residues involved in the binding to haem of IsdG are depicted as magenta stick models and labelled. The overlapping residues of Isd-LmHde are also represented as green stick models and labelled. Haem and all residues are coloured by element with carbon in yellow (haem), green (IsdG) or magenta (Isd-LmHde), oxygen in red and nitrogen in blue. The iron of the haem molecule is coloured light red and labelled. (*d*) Structural alignment: the ribbon diagrams of Isd-LmHde, HmoB and IsdG, depicted in wheat, cyan and violet, respectively, show that a flexible region is close to the haem-binding site. The loop of the IsdG–haemin structure (Asp71–Ser88), which is disordered in the apo IsdG structure, is coloured green. The corresponding region in Isd-LmHde (Lys131–Lys144) is coloured blue. The corresponding region in apo HmoB (Gly138–Thr156) is also disordered and each terminus of this region is coloured red. Haem is depicted as a yellow stick model. Isd-LmHde, HmoB and IsdG are compared by surface presentation with haem in the same orientation and colour scheme as in the structural alignment. The haems in Isd-LmHde and HmoB are modelled based on the structural overlap with IsdG.

that Lmo2213 is a putative haem-degrading enzyme in *L. monocytogenes* as a HmoB or IsdG homologue, and thus designated it as Isd-LmHde (IsdG-type haem-degradation enzyme).

3.2. Overall structure of Isd-LmHde

The crystal structure of Isd-LmHde was determined at 1.75 Å resolution with R_{work} and R_{free} factors of 18.8 and 24.4%, respectively. Residues 44–49 and 161–167 were not modelled, probably owing to weak electron density, and thus the current model comprises residues 1–43 and 50–160 together with 177 water molecules. The average *B* factor of the structure is 16.24 Å^2 and no residues are outliers as validated by the Ramachandran plot statistics (Table 1). There is one protein subunit per asymmetric unit. Isd-LmHde consists of an antiparallel β-barrel surrounded by four α-helices (Fig. 2*a*). Isd-LmHde is divided into N- and C-terminal domains (Fig. 2*b*); the N-terminal domain has one helix (α1) packed against a four-stranded β-sheet (Fig. 2*b*) and the C-terminal domain has a β5–α2–β6–β7–α3–α4–β8 topology that belongs to the ferredoxin-like fold according to the SCOP

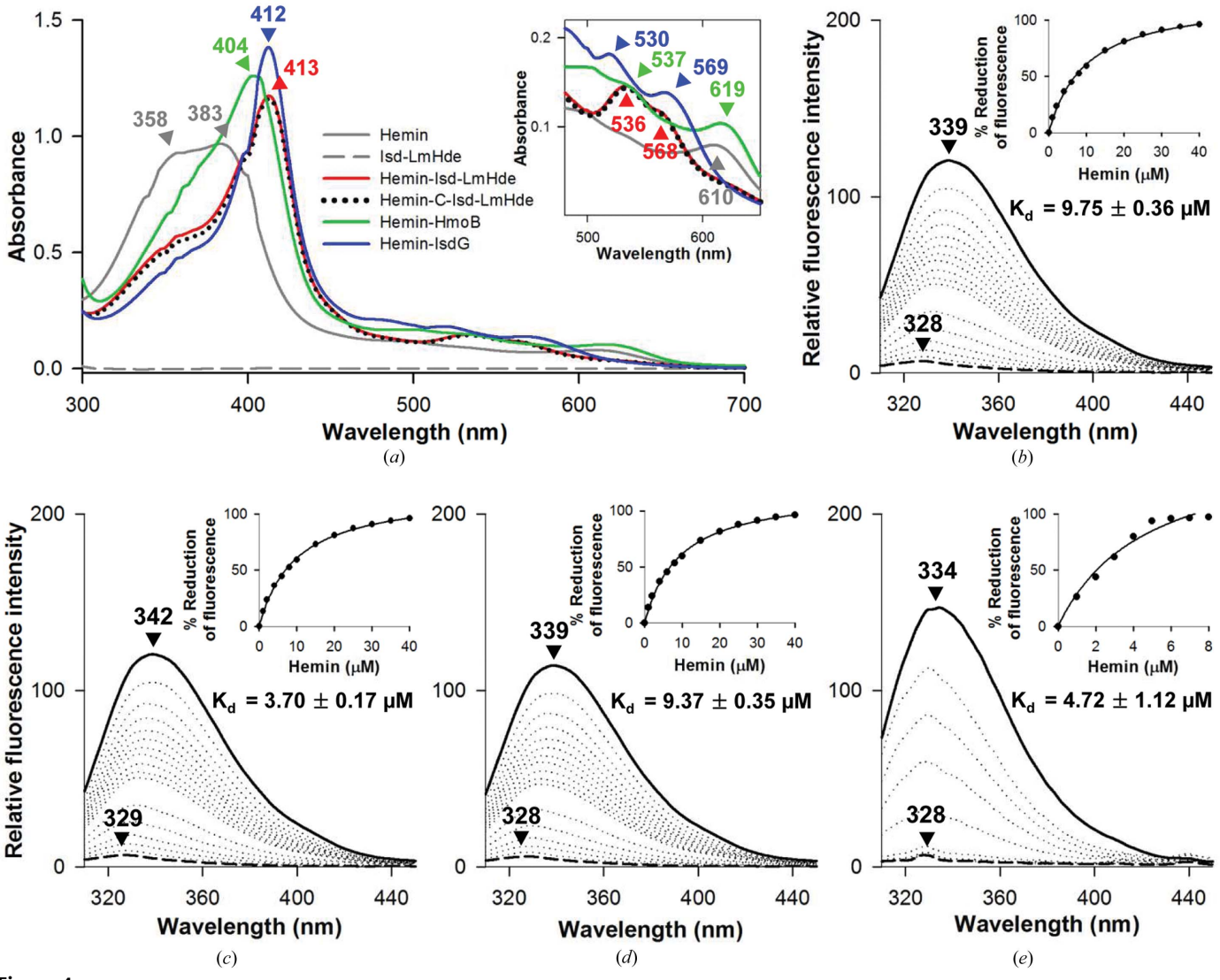

Figure 4
Haem-binding activity of Isd-LmHde, HmoB and IsdG. (*a*) Absorption spectra of haemin bound to intact Isd-LmHde, C-Isd-LmHde, HmoB and IsdG. The spectrum of the haemin–Isd-LmHde complex is shown as a solid red line, that of the haemin-C-Isd-LmHde complex as a dotted black line, that of the haemin–HmoB complex as a solid green line, that of the haem–IsdG complex as a solid blue line, that of haemin as a solid grey line and that of apo Isd-LmHde as a dashed grey line. The triangles in the respective colours indicate the maximum peaks of each spectrum and the corresponding wavelengths (in nm) are labelled above the black triangles. The inset shows a magnification of the absorption spectra in the wavelength range 480–650 nm. Fluorescence spectra of haemin binding to (*b*) Isd-LmHde, (*c*) HmoB and (*d*) IsdG. Haemin was added to 5 μ*M* protein in increments of 1 μ*M* up to 40 μ*M* haemin. The spectrum before addition of haemin is shown as a solid line, spectra for every addition of haemin are shown as dotted lines and the spectrum with 40 μ*M* haemin is shown as a dashed line. The black triangles indicate the maximum peaks of each spectrum and the corresponding wavelengths (in nm) are labelled above the black triangles. Inset, titration curve for the incremental addition of haemin *versus* the quenched fluorescence intensity at 339 nm (Isd-LmHde), 342 nm (HmoB), 339 nm (C-Isd-LmHde) or 339 nm (IsdG). The curve was fitted using *SigmaPlot* to the theoretical curve of the indicated K_d value.

classification (Lo Conte *et al.*, 2002; Fig. 2*b*). Atomic coordinates and structure-factor amplitudes of Isd-LmHde have been deposited in the PDB as entry 4kia.

The overall fold of Isd-LmHde is similar to that of *B. subtilis* HmoB, with a root-mean-square deviation (r.m.s.d) of 2.1 Å for 124 C^{α} atoms (Fig. 2*c*). The C-terminal domain of Isd-LmHde (C-Isd-LmHde) has a similar fold to one monomer of IsdG and IsdI from *S. aureus*. However, their structural similarity is not as high as that between Isd-LmHde and HmoB: the r.m.s.d. values of Isd-LmHde with IsdG and IsdI are 4.0 Å for 72 C^{α} atoms and 5.6 Å for 75 C^{α} atoms, respectively (Fig. 2*c*). Isd-LmHde has an extra N-terminal domain that is not present in IsdG and IsdI. The N-terminal domain of Isd-LmHde can be considered as a pseudo-ferredoxin-like fold that lacks the second helix between β3 and β4. From this analysis, it is tempting to propose that the Isd-LmHde monomer has a fold similar to that of a homodimeric β-barrel fold of IsdG. As it is, the N-terminal and C-terminal domains of Isd-LmHde can be superimposed on each subunit of the IsdG dimer, respectively (Fig. 2*c*).

Isd-LmHde has eight antiparallel β-strands in the centre which are surrounded by one α-helix on one side and three α-helices on the opposite side (Fig. 2*a*). The central eight-stranded β-barrel is maintained by hydrophobic interactions between four β-strands from the N-terminal domain and four from the C-terminal domain (Fig. 3*a*). The IsdG dimer also forms an eight-stranded β-barrel, which similarly consists of four β-strands from one subunit and four β-strands from the other subunit and is stabilized by hydrophobic interactions (Fig. 3*b*). Therefore, the N-terminal and C-terminal domains of Isd-LmHde pack together in a similar way as the two subunits in the IsdG dimer.

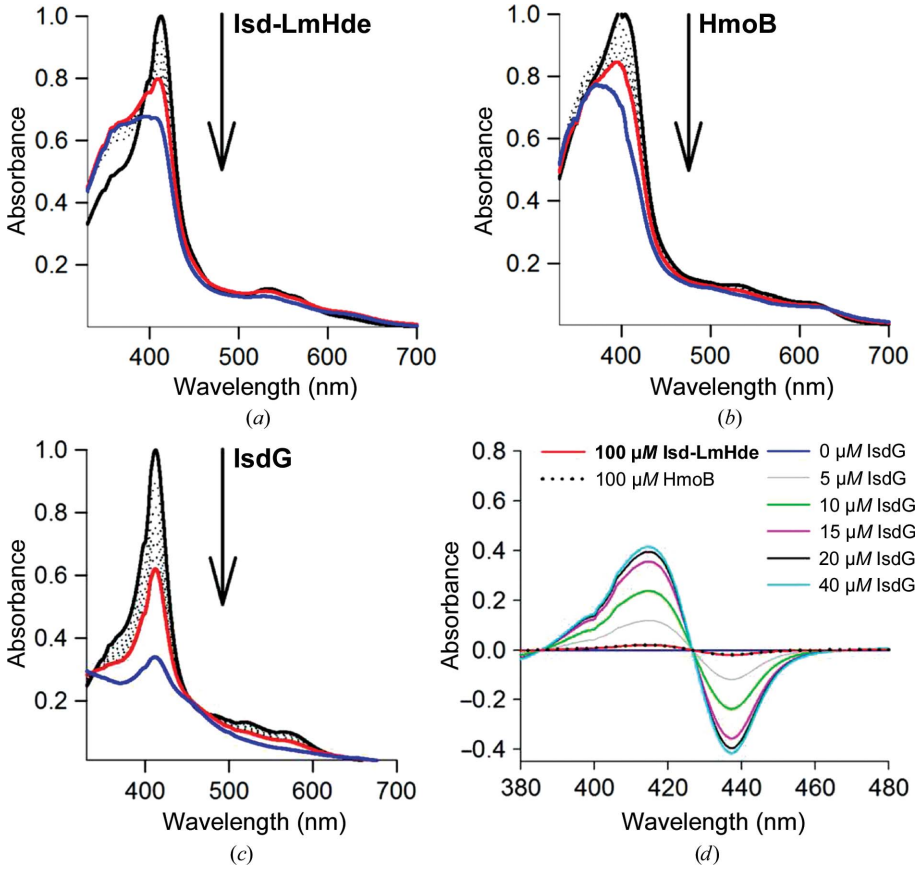

Figure 5
Haem-degradation activity of Isd-LmHde, HmoB and IsdG and detection of CO. Absorption spectra of haem degradation in the presence of (*a*) Isd-LmHde, (*b*) HmoB and (*c*) IsdG. Absorption spectra of the haemin–protein complex at 10 µ*M* were measured in the presence of ascorbic acid and catalase at a molar ratio of 0.5:1.0 (catalase:haemoprotein). The spectrum before the addition of ascorbic acid is shown as a solid black line. The spectra of intermediate time points (every 5 min) after the addition of ascorbic acid are shown as dotted lines. The spectrum at 30 min is shown as a solid red line and the spectrum at 2 h is shown as a solid blue line. The arrow indicates the direction of movement over the course of 2 h. The maximum absorption value was normalized to 1.0 for clearer comparison. (*d*) Detection of CO generated from the haem-degradation reaction. Absorption spectra of myoglobin bound to CO were drawn by subtracting the control spectrum from the absorption spectra of myoglobin with the product of the haem-degradation reaction by IsdG at various concentrations (0–40 µ*M*), 100 µ*M* HmoB and 100 µ*M* Isd-LmHde. Control spectra were obtained from the reaction mixture before haem degradation. Each spectrum is indicated by different colours in the box. The spectral change accompanying the reaction product of IsdG is proportional to the concentration of IsdG, indicating that the concentration of the generated CO was increased by IsdG. However, no spectral change was observed when HmoB or Isd-LmHde was used, suggesting that CO was not generated during haem degradation by HmoB or Isd-LmHde.

3.3. Haem-binding activity of Isd-LmHde

Structural comparison of Isd-LmHde with HmoB and IsdG raises the possibility that Isd-LmHde might have a similar functionality to HmoB or IsdG. However, of the residues of the Asn-Trp-His catalytic triad that is essential for haem monoxygenase activity found in IsdG (Wu *et al.*, 2005) and HmoB (Gaballa & Helmann, 2011), only Trp is conserved in Isd-LmHde (Fig. 1*b*). Thus, an intriguing question is whether Isd-LmHde also degrades haem and, if so, by what reaction mechanism.

The interaction between Isd-LmHde and haemin was investigated by monitoring the reconstitution of the haemin–protein complex using ultraviolet–visible (UV–Vis) and fluorescence spectroscopy. The reconstituted haemin–protein complex typically shows a Soret peak near 400–415 nm and broad peaks near 530–545 and 560–580 nm (Wilks & Schmitt, 1998; Suits *et al.*, 2005; Skaar *et al.*, 2004). Consistently, the reconstituted haemin with Isd-LmHde showed the Soret peak at 413 nm and broad peaks at 536 and 568 nm, while haemin showed absorbance maxima at 358 and 383 nm (Fig. 4*a*). However, Isd-LmHde alone showed no detectable absorbance in the same wavelength range, proving that the Soret peak originated not from

protein but from haem (Fig. 4*a*). Additionally, the visible spectrum of haemin reconstituted with Isd-LmHde is quite different from those with HmoB or IsdG; the haemin–HmoB complex has a Soret peak at 404 nm and a broad peak at 537 and 619 nm and the haemin–IsdG complex has a Soret peak at 412 nm and broad peaks at 530 and 569 nm (Fig. 4*a*). The difference in the optical absorption spectra between haemin–Isd-LmHde and haemin–IsdG indicates the dissimilarity in the haem environment between Isd-LmHde and IsdG. Collectively, the spectroscopic analyses of the haemin–protein complex confirmed the binding of haemin to Isd-LmHde.

Since the haem-binding pocket in IsdG has been defined by structural and functional studies (Wu *et al.*, 2005; Lee *et al.*, 2008), a putative haem-binding site in Isd-LmHde can be predicted from the structural overlap between Isd-LmHde and IsdG (Fig. 3*c*). From the structural alignment, haem binding is expected to cause fluorescence quenching of Trp129, since this residue is located near the putative haem-binding site of Isd-LmHde (Fig. 3*c*). Therefore, the binding of haem to Isd-LmHde was also investigated by the quenching of the intrinsic fluorescence of Isd-LmHde upon haemin titration. Haemin was incrementally added to apoprotein and the intrinsic Trp fluorescence of Isd-LmHde was monitored. An excitation wavelength of 295 nm was chosen to minimize the interference of Tyr and Phe. The spectra showed that the magnitude of Trp fluorescence gradually decreased as the amount of haemin increased, and the emission-peak maximum was blue-shifted from 339 to 328 nm, indicating that haemin binds Isd-LmHde near the Trp residue (Fig. 4*b*). Comparably, HmoB and IsdG also showed similar fluorescence quenching in the presence of haemin, and the maximal peaks of the emission spectra were shifted from 342 to 329 nm and from 334 to 328 nm, respectively (Figs. 4*c* and 4*e*). The reduction in the relative fluorescence intensity of Trp at the wavelengths of the maximal peaks (*i.e.* 339 nm for Isd-LmHde, 342 nm for HmoB and 334 nm for IsdG) were plotted against the haemin concentration to calculate the haem-binding affinity in terms of the dissociation constant (K_d) of each protein. The results showed that the K_d values of Isd-LmHde, HmoB and IsdG for haemin are 9.75 $\pm$ 0.36, 3.70 $\pm$ 0.17 and 4.72 $\pm$ 1.12 μM, respectively (insets in Figs. 4*b*, 4*c* and 4*e*). The calculated K_d value of IsdG for haemin is consistent with the reported K_d value of 5.0 $\pm$ 1.5 μM (Skaar *et al.*, 2004).

3.4. Haem-degrading activity of Isd-LmHde

The haem-degradation activity of Isd-LmHde was monitored by the reduction of the Soret peak of the haemin–protein complex (Skaar *et al.*, 2004). Initially, several reductants were screened as electron donors to optimize the reaction conditions of Isd-LmHde (Supplementary Fig. S1). Among them, ascorbic acid turned out to work best in Isd-LmHde-catalyzed haem degradation and thus ascorbic acid was used for the activity assay of Isd-LmHde. After a 30 min incubation with haemin and Isd-LmHde in the reaction buffer, it was confirmed that the Soret peak was reduced by 21.3% (Fig. 5*a*), which is comparable to the peak reduction caused by HmoB in the same reaction condition (19.1%; Fig. 5*b*) but is lower than that caused by IsdG (37.9%; Fig. 5*c*). Isd-LmHde degraded haem by a further 37% after a 2 h incubation (Fig. 5*a*).

Conclusively, Isd-LmHde binds and degrades haem, but it lacks the key catalytic Asp and His which are known to be essential in IsdG (Wu *et al.*, 2005) and HmoB (Gaballa & Helmann, 2011). To elucidate the mode of haem degradation by Isd-LmHde, the reaction products were analyzed using MALDI–TOF mass spectrometry. In the MALDI–TOF spectra acquired after 1 and 3 h of haem degradation, two abundant peaks arose at m/z = 583.3 and 616.2, which match the m/z values of biliverdin (exact mass 583.2557 Da, protonated form) and haem (exact mass 616.1773, protonated form), respectively (Fig. 6). In Fig. 6, it is clearly shown that as the reaction continued the amount of haem which was degraded into biliverdin by Isd-LmHde increased.

Since CO is generated as a product, together with biliverdin, of most known haem-degrading enzymes, we examined CO production from the haem-degradation reaction conducted by Isd-LmHde in order to understand its reaction mechanism. CO production was monitored by the binding of the generated CO to myoglobin, which causes a blue shift of the Soret peak from 434 to 423 nm (Iizuka *et al.*, 1974). CO generation from the haem degradation catalyzed by IsdG was used as a positive control, although it produces CO with a low yield (Matsui *et al.*, 2013). The sensitivity of the CO-detection assay was determined using varying concentrations of IsdG. It was shown that 10 μM dithionite-reduced myoglobin could detect the CO produced in a 1 h reaction catalyzed by 5 μM IsdG (Fig. 5*d*). The difference absorbance in the Soret region of the

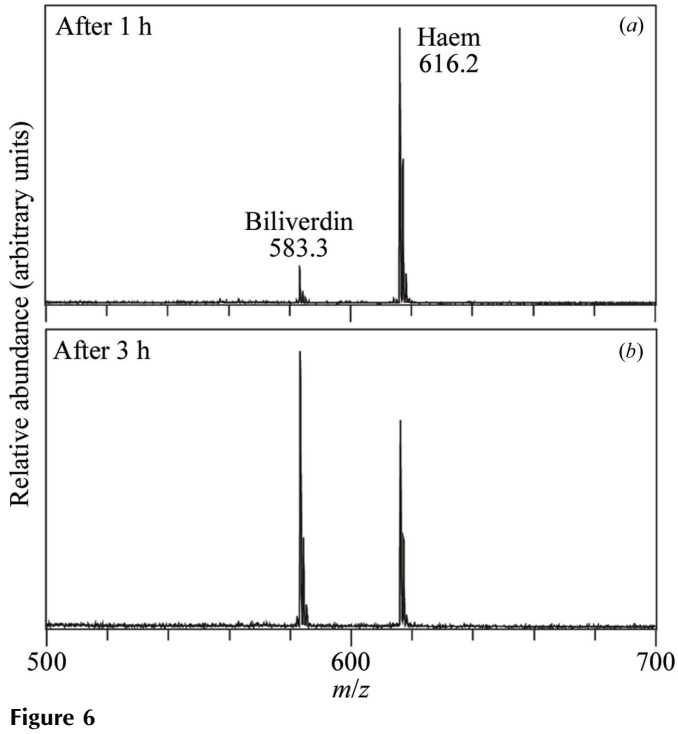

Figure 6
Haem-degradation products using Isd-LmHde. MALDI-TOF mass spectra acquired after 1 h (*a*) and 3 h (*b*) of haem degradation.

Table 2
Haem-degrading activity of Isd-LmHde and its mutants.

The reduction in the haem-degrading activity of the mutants in comparison to the wild type is presented as a percentage.

Protein	Reduction of haem-degrading activity (%)
Wild type	0
C-Isd-LmHde	67.92
Y53A	0.53
E71A	36.16
I73R	28.93
Y87A	36.96
F126R	24.81
W129R	61.87
W129A	64.63
S135A	21.85
T139A	25.51
M142A	24.81

difference spectrum of CO-bound myoglobin that was generated by 5 μ*M* IsdG was comparable to the reported value (about 0.1; Matsui *et al.*, 2013). However, the myoglobin-based assay hardly detected CO liberation when even 100 μ*M* Isd-LmHde or HmoB were used in the same conditions (Fig. 5*d*). If Isd-LmHde shows the same activity as IsdG, approximately 20 μ*M* CO would be expected to be released from 100 μ*M* Isd-LmHde. Thus, it was concluded that the CO released from haem degradation by Isd-LmHde or HmoB is very much less than that released by IsdG.

3.5. Key residues involved in haem binding and degradation by Isd-LmHde

In order to understand the haem-binding mode and catabolic mechanism of Isd-LmHde at the molecular level, a high-resolution structure of the haem–protein complex would be necessary. However, co-crystallization of a Isd-LmHde–haemin complex or soaking of haemin into Isd-LmHde crystals was not successful, probably owing to the structural heterogeneity of the haem-bound Isd-LmHde. Therefore, site-directed mutagenesis was employed to elucidate the key residues for binding and activity. Based on the structural similarity of Isd-LmHde to IsdG and HmoB, the haem-binding site of Isd-LmHde was predicted (Fig. 3*c*). Notably, the loop comprising Asp71–Ser88, which forms one side of the haem-binding cleft, is disordered in the apo form of IsdG but is stabilized in the presence of haem. Moreover, the corresponding loop of apo HmoB (Gly138–Thr156) is also not modelled in the crystal structure. Therefore, it is hypothesized that the haem-binding cleft is remodelled by the entry of haem (Lee *et al.*, 2008). In the case of Isd-LmHde, the corresponding region (Lys131–Lys144) forms a well ordered helix but partially blocks the haem-binding cleft (Fig. 3*d*). Therefore, it is assumed that the haem-binding pocket in the current crystal structure can be opened by the movement of the helix upon haem binding. By structural overlap, key residues of IsdG essential for haem binding and degradation were aligned with the corresponding residues in Isd-LmHde (Fig. 3*c*). Among them, Ile73, Tyr87, Phe126 and Trp129, which are also highly conserved in the sequence alignment (Fig. 1*b*), were mutated to Arg or Ala to examine their roles in the haem-binding and degradation activity. However, no detectable change in the haem-binding activity was observed compared with wild-type Isd-LmHde (Supplementary Table S3). Since the haem-binding pocket is built by many residues, a single mutation might not affect the interaction of Isd-LmHde with haem. Consistently, a single mutation in the haem-binding pocket did not alter the haem-binding activity in the cases of IsdG, IsdI (Wu *et al.*, 2005) and HmoB (Gaballa & Helmann, 2011).

The haem-degradation activity of the mutants was then investigated. For this purpose, Glu71 and Ser135 were also mutated to Ala since these residues superimpose on two critical residues in the catalytic triad of IsdG (Asn7 and His77; Figs. 1*b* and 3*c*). However, it is worth noting that structure comparison between apo and haem-bound IsdG revealed that among the residues involved in haem binding, only His77 moves upon haem binding. Thus, only a few residues of Isd-LmHde might be affected by haem-induced structural rearrangements. Accordingly, we expected that Ser135, which superimposes on the catalytic residue His77 in IsdG, might move away upon haem binding, but that most of the putative haem-binding residues would be virtually unaffected (Figs. 1*b* and 3*c*). In this regard, T139A and M142A mutants were also produced since they might be able to overlap with His77 of IsdG in the haem-bound Isd-LmHde.

Among the tested mutants, W129A or W129R, which are mutants of the key residues in the catalytic triad of IsdG, showed the most striking reduction in haem-degrading activity (Table 2 and Supplementary Fig. S2). The haem-degrading activity of Isd-LmHde was also affected by mutation of Glu71, the residue corresponding to the second key residue (Asn7 in IsdG), and mutation of Ser135, the residue that superimposes on the third key residue (His77 of IsdG), being reduced by 36.2 and 21.9%, respectively (Table 2 and Supplementary Fig. S2). Surprisingly, Isd-LmHde Y87A showed a significant reduction in haem-degrading activity similar to that of the E71A mutant (37.0%; Table 2 and Supplementary Fig. S2). Other mutants also showed decreased activity, but the decrease was within the range 24–28% (Table 2 and Supplementary Fig. S2). Since there was no detectable change in their CD spectra (Supplementary Fig. S3), the reduced haem-degrading activity of the mutants seems not to be caused by a folding defect, but rather by mutations near the haem-binding site. It is worth noting that the mutation of a residue which is not located in the putative haem-binding pocket, such as Tyr53, did not affect the haem-degrading activity of Isd-LmHde (Table 2 and Supplementary Fig. S2). Thus, among the residues identified from the site-directed mutagenesis and haem-degrading assay, all appear to contribute to haem degradation but to variable extents. That is, Trp129 is considered to be the most important residue, followed by Glu71 and Tyr87 (Table 2 and Supplementary Fig. S2).

3.6. The role of the N-terminal domain of Isd-LmHde

The most notable difference from IsdG is the presence of an extra N-terminal domain in Isd-LmHde. To investigate the

contribution of each domain, the N-terminal (Met1–Gly50) and C-terminal (Ala51–Lys167) domains were separately expressed. However, the expression of the N-terminal truncation mutant was hampered by low stability. Interestingly, the C-terminal domain (C-Isd-LmHde; residues 51–167) forms a homogenous homodimer in solution like the IsdG protein, whereas full-length Isd-LmHde is monomeric (Supplementary Fig. S4). Full-length Isd-LmHde and C-Isd-LmHde have similar haem-binding abilities and the same spectral properties characterized by a Soret peak at 413 nm and broad peaks at 536 and 568 nm (Fig. 4*a*). In addition, the Trp fluorescence of C-Isd-LmHde as well as the full-length protein was similarly quenched by haemin (Fig. 4*d*). Accordingly, the haemin-binding affinity of C-Isd-LmHde is also comparable to that of the full-length protein: K_d for C-Isd-LmHde–haemin is 9.37 ± 0.35 μ*M* and K_d for intact Isd-LmHde–haemin is 9.75 ± 0.36 μ*M* (insets in Figs. 4*b* and 4*d*). However, the haem-degradation activity of C-Isd-LmHde was drastically reduced (Table 2 and Supplementary Fig. S2). These results suggest that the N-terminal domain is related to catalytic function rather than haem binding.

4. Discussion

In this study, we first identified an IsdG-type haem-degradation enzyme from *L. monocytogenes* EGD-e by structural and biochemical characterization and designated it as Isd-LmHde (formerly Lmo2213). While we were working on this protein, the coordinates of its homologue from *L. monocytogenes* 4b F2365 were deposited in the PDB as part of a structural genomics project (PDB entry 3fez). The structures share high sequence identity (98.2%) and structural similarity (r.m.s.d. of 0.50 Å for 121 C^{α} atoms), but 3fez was designated as an 'uncharacterized ferredoxin-fold protein related to antibiotic biosynthesis monooxygenases' without biochemical characterization. Therefore, our study is the first characterization of this protein as a haem-degrading enzyme in *L. monocytogenes*.

Isd-LmHde has a similar fold to previously identified haem-degrading enzymes from Gram-positive bacteria, such as IsdG and HmoB (Fig. 2*c*), and shows a comparable haem-binding activity (Fig. 4). The haem-degradation activity of Isd-LmHde is comparable to that of HmoB, although it is not as efficient as IsdG (Fig. 5). In this study, haem degradation by Isd-LmHde was monitored by the reduction of the Soret peak (Fig. 5). The Soret peak of the haemoprotein complex was only reduced in the presence of an electron-donor source (Supplementary Fig. S1), which supports the premise that the reduction of the Soret peak is caused by the catalytic activity of Isd-LmHde, rather than by the dissociation of haem from Isd-LmHde. It is also evident that haem was degraded in the enzymatic reaction catalyzed by Isd-LmHde since the degradation assay was performed in the presence of catalase in order to eliminate non-enzymatic degradation by hydrogen peroxide *via* a coupled oxidation reaction (Sigman *et al.*, 2001).

IsdG (Wu *et al.*, 2005) and HmoB (Gaballa & Helmann, 2011) commonly have three conserved residues, Asn-Trp-His, that are essential for haem degradation. Among the three key residues in the catalytic triad of IsdG, Trp67 is known to cause the ruffling of haem which is necessary for its degradation (Lee *et al.*, 2008; Ukpabi *et al.*, 2012). His77 serves as the haem axial ligand (Reniere *et al.*, 2010; Wu *et al.*, 2005) and Asn7 is essential for enzymatic activity by performing two roles in catalysis (Lee *et al.*, 2008; Reniere *et al.*, 2010; Wu *et al.*, 2005): (i) forming a hydrogen bond to the bound oxygen species to stabilize the reaction intermediate (Lee *et al.*, 2008) and (ii) contributing to the distortion of the porphyrin ring (Lee *et al.*, 2008). In addition, Phe23 in IsdG was also proposed to play a role in directing haem ruffling (Lee *et al.*, 2008). Among the residues in the catalytic triad, only Trp is conserved in the sequence and structure of Isd-LmHde (Figs. 1*b* and 3*c*). Accordingly, substitution of Trp129 by Ala or Arg significantly reduced the haem-degrading activity of Isd-LmHde, and the reduction of haem degradation by the W129A mutant (64.6%) is little greater than that by the W129R mutant (61.9%) (Table 2 and Supplementary Fig. S2). It is suggested that the presence of a smaller side chain at position 129 results in lower haem-degradation activity, which can be explained by an impaired haem ruffling. Although Isd-LmHde lacks the catalytic Asn, Glu71, which structurally overlaps with Asn7 of IsdG (Fig. 3*c*), also seems to play a role in haem degradation, since its mutation to Ala reduced the degradation activity. However, Isd-LmHde does not appear to have a residue corresponding to His77, since the mutation of Ser135, Thr139 and Met142, which might functionally replace His, showed only marginal changes in activity (Table 2 and Supplementary Fig. S2). Interestingly, Tyr87, which structurally overlaps with Phe23 of IsdG, is likely to be involved in haem degradation because its mutation reduced the activity to a similar extent to that of Glu71. Taking these results together, the reduced degradation activity of Isd-LmHde W129A, Y87A and E71A can be explained by impaired haem ruffling. In this regard, it can be proposed that the haem-distortion step is necessary for haem degradation in Isd-LmHde as in IsdG and HmoB. However, it seems that Isd-LmHde is distinctive from the known IsdG-family enzymes in that it lacks the Asn and His or their functional substitutes which are known to bind dioxygen and iron, respectively, in the catalysis of haem monooxygenases.

The results of MALDI–TOF mass spectrometry demonstrated that Isd-LmHde generates biliverdin as a product of haem degradation, as known for the HO-like family and the ChuS family (Fig. 6). In addition, we confirmed that Isd-LmHde and HmoB do not produce CO or produce considerably smaller amounts of CO (Fig. 5*d*), while the HO-like family and the ChuS family produce CO (Wilks & Schmitt, 1998; Suits *et al.*, 2005), which suggests that they have different mechanisms of haem degradation. MhuD from *M. tuberculosis* has recently been reported to degrade haem to mycobilin without generating CO, possibly through a novel mechanism (Nambu *et al.*, 2013). However, MhuD was shown to be similar to IsdG and IsdI in its active-site structure and in its requirement for haem ruffling for degradation (Nambu *et al.*, 2013). It was noted that IsdG produces CO with a low yield of

about 14%, but Isd-LmHde or HmoB seem to produce much less CO than IsdG. Moreover, in terms of residues in the active site, Isd-LmHde is distinguishable from IsdG or HmoB. These results suggest that their catalytic mechanisms are different, which should be elucidated in further structural analyses.

Structurally, C-Isd-LmHde resembles full-length IsdG or IsdI, and the monomeric form of Isd-LmHde is similar to the IsdG dimer (Fig. 2*c*). From these findings, we assumed that C-Isd-LmHde alone may act as a haem-degradation enzyme, and characterized the biochemical properties of C-Isd-LmHde. Interestingly, C-Isd-LmHde forms a dimer, while intact Isd-LmHde exists as a monomer (Supplementary Fig. S4). Furthermore, C-Isd-LmHde possesses a haem-binding affinity comparable to that of intact Isd-LmHde (Figs. 4*b* and 4*d*). Its catalytic activity, however, was much weaker (Table 2 and Supplementary Fig. S2). This can be interpreted as that the C-terminal domain may be functionally analogous to the single subunit of IsdG in terms of haem binding, but the N-terminal domain is critical for the catalytic activity of Isd-LmHde *via* proper formation of the catalytic site.

We thank Tri Ngo for assistance with docking simulations and Kyunghee Yun for assistance with site-directed mutagenesis. We also thank Doyoun Kim for helping to solve the structure. We are grateful for the kind support from Agilent Technologies in Korea in providing a demo version of the C18 column. This work was supported by National Research Foundation of Korea (NRF) grant (2011-0028878).

References

Adams, T. J., Vartivarian, S. & Cowart, R. E. (1990). *Infect. Immun.* **58**, 2715–2718.

Anzaldi, L. L. & Skaar, E. P. (2010). *Infect. Immun.* **78**, 4977–4989.

Armstrong, R. W. & Fung, P. C. (1993). *Clin. Infect. Dis.* **16**, 689–702.

Bradford, M. M. (1976). *Anal. Biochem.* **72**, 248–254.

Cole, C., Barber, J. D. & Barton, G. J. (2008). *Nucleic Acids Res.* **36**, W197–W201.

Conte, M. P., Longhi, C., Polidoro, M., Petrone, G., Buonfiglio, V., Di Santo, S., Papi, E., Seganti, L., Visca, P. & Valenti, P. (1996). *Infect. Immun.* **64**, 3925–3929.

Emsley, P. & Cowtan, K. (2004). *Acta Cryst.* D**60**, 2126–2132.

Farber, J. M. & Peterkin, P. I. (1991). *Microbiol. Rev.* **55**, 476–511.

Gaballa, A. & Helmann, J. D. (2011). *Microbiology*, **157**, 3221–3231.

Gouet, P., Courcelle, E., Stuart, D. I. & Métoz, F. (1999). *Bioinformatics*, **15**, 305–308.

Gray, M. L. (1962). *Ann. N. Y. Acad. Sci.* **98**, 686–699.

Hammer, N. D. & Skaar, E. P. (2011). *Annu. Rev. Microbiol.* **65**, 129–147.

Hartford, T., O'Brien, S., Andrew, P. W., Jones, D. & Roberts, I. S. (1993). *FEMS Microbiol. Lett.* **108**, 311–318.

Holland, S., Alfonso, E., Gelender, H., Heidemann, D., Mendelsohn, A., Ullman, S. & Miller, D. (1987). *Cornea*, **6**, 144–146.

Iizuka, T., Yamamoto, H., Kotani, M. & Yonetani, T. (1974). *Biochim. Biophys. Acta*, **371**, 126–139.

Jin, B., Newton, S. M. C., Shao, Y., Jiang, X., Charbit, A. & Klebba, P. E. (2006). *Mol. Microbiol.* **59**, 1185–1198.

Lansky, I. B., Lukat-Rodgers, G. S., Block, D., Rodgers, K. R., Ratliff, M. & Wilks, A. (2006). *J. Biol. Chem.* **281**, 13652–13662.

Laskowski, R. A., MacArthur, M. W., Moss, D. S. & Thornton, J. M. (1993). *J. Appl. Cryst.* **26**, 283–291.

Lee, W. C., Reniere, M. L., Skaar, E. P. & Murphy, M. E. P. (2008). *J. Biol. Chem.* **283**, 30957–30963.

Lo Conte, L., Brenner, S. E., Hubbard, T. J. P., Chothia, C. & Murzin, A. G. (2002). *Nucleic Acids Res.* **30**, 264–267.

Matsui, T., Nambu, S., Ono, Y., Goulding, C. W., Tsumoto, K. & Ikeda-Saito, M. (2013). *Biochemistry*, **52**, 3025–3027.

Morris, R. J., Perrakis, A. & Lamzin, V. S. (2003). *Methods Enzymol.* **374**, 229–244.

Murshudov, G. N., Skubák, P., Lebedev, A. A., Pannu, N. S., Steiner, R. A., Nicholls, R. A., Winn, M. D., Long, F. & Vagin, A. A. (2011). *Acta Cryst.* D**67**, 355–367.

Nambu, S., Matsui, T., Goulding, C. W., Takahashi, S. & Ikeda-Saito, M. (2013). *J. Biol. Chem.* **288**, 10101–10109.

Newton, S. M. C., Klebba, P. E., Raynaud, C., Shao, Y., Jiang, X., Dubail, I., Archer, C., Frehel, C. & Charbit, A. (2005). *Mol. Microbiol.* **55**, 927–940.

Otwinowski, Z. & Minor, W. (1997). *Methods Enzymol.* **276**, 307–326.

Park, S., Choi, S. & Choe, J. (2012). *BMB Rep.* **45**, 239–241.

Puri, S. & O'Brian, M. R. (2006). *J. Bacteriol.* **188**, 6476–6482.

Rabau, E. & David, A. (1962). *Harefuah*, **62**, 41–43.

Reniere, M. L., Torres, V. J. & Skaar, E. P. (2007). *Biometals*, **20**, 333–345.

Reniere, M. L., Ukpabi, G. N., Harry, S. R., Stec, D. F., Krull, R., Wright, D. W., Bachmann, B. O., Murphy, M. E. & Skaar, E. P. (2010). *Mol. Microbiol.* **75**, 1529–1538.

Schuller, D. J., Wilks, A., Ortiz de Montellano, P. R. & Poulos, T. L. (1999). *Nature Struct. Mol. Biol.* **6**, 860–867.

Schuller, D. J., Zhu, W., Stojiljkovic, I., Wilks, A. & Poulos, T. L. (2001). *Biochemistry*, **40**, 11552–11558.

Sigman, J. A., Wang, X. & Lu, Y. (2001). *J. Am. Chem. Soc.* **123**, 6945–6946.

Simon, N., Coulanges, V., Andre, P. & Vidon, D. J. (1995). *Appl. Environ. Microbiol.* **61**, 1643–1645.

Sinclair, P. R., Gorman, N. & Jacobs, J. M. (2001). *Curr. Protoc. Toxicol.*, Unit 8.3. doi:10.1002/0471140856.tx0803s00.

Skaar, E. P., Gaspar, A. H. & Schneewind, O. (2004). *J. Biol. Chem.* **279**, 436–443.

Suits, M. D. L., Pal, G. P., Nakatsu, K., Matte, A., Cygler, M. & Jia, Z. (2005). *Proc. Natl Acad. Sci. USA*, **102**, 16955–16960.

Sword, C. P. (1966). *J. Bacteriol.* **92**, 536–542.

Thompson, J. D., Higgins, D. G. & Gibson, T. J. (1994). *Nucleic Acids Res.* **22**, 4673–4680.

Ukpabi, G., Takayama, S. J., Mauk, A. G. & Murphy, M. E. P. (2012). *J. Biol. Chem.* **287**, 34179–34188.

Unno, M., Matsui, T. & Ikeda-Saito, M. (2007). *Nat. Prod. Rep.* **24**, 553–570.

Unno, M., Matsui, T. & Ikeda-Saito, M. (2012). *J. Inorg. Biochem.* **113**, 102–109.

Vagin, A. & Teplyakov, A. (2010). *Acta Cryst.* D**66**, 22–25.

Whitelock-Jones, L., Carswell, J. & Rasmussen, K. C. (1989). *S. Afr. Med. J.* **75**, 188–189.

Wilks, A. & Schmitt, M. P. (1998). *J. Biol. Chem.* **273**, 837–841.

Wu, R., Skaar, E. P., Zhang, R., Joachimiak, G., Gornicki, P., Schneewind, O. & Joachimiak, A. (2005). *J. Biol. Chem.* **280**, 2840–2846.